MADRID
inter.noise 2019
June 16 - 19
NOISE CONTROL FOR A BETTER ENVIRONMENT

# Low-frequency sound absorber based on checkerboard Helmholtz resonators with different extended necks

**Guo, Jingwen**[1]
**Department of Mechanical and Aerospace Engineering, Hong Kong University of Science and Technology, Clear Water Bay, Kowloon, Hong Kong**

**Zhang, Xin** [2]
**Department of Mechanical and Aerospace Engineering, Hong Kong University of Science and Technology, Clear Water Bay, Kowloon, Hong Kong**

## ABSTRACT

**In this study, we develop a checkerboard sound absorber based on Helmholtz resonator with extended neck (HREN), which is capable of low-frequency noise reduction. The absorber is constructed of alternating HRENs with varying-length extended necks. Based on the transfer matrix method coupled with the equivalent medium method, an analytical model is developed to predict the sound absorption characteristics of the absorber. Its accuracy is validated by the experimental measurements in an impedance tube. Then, we report an analytical and experimental study on the absorption characteristics of HRENs and the checkerboard sound absorbers. Results show that HREN is featured by its thin thickness, and its resonance frequency can be flexibly tuned by designing the length of the extended neck. It is found that the coupling between resonators becomes quite weak if two adjacent resonators in a checkerboard absorber are largely dissimilar. In this case, they operate almost independently, resulting in a dual-band sound absorption performance. A wide-bandwidth absorber can be obtained if two adjacent resonators in the checkerboard absorber are strong coupling. The wide-bandwidth absorber exhibits a quasi-perfect absorption (the absorption coefficient above 0.9) in a wide bandwidth between two absorption peaks induced by two corresponding uniform HRENs. Both the dual-band and wide-bandwidth absorbers still possess the feature of sub-wavelength scale thickness. The proposed checkerboard absorber holds promising potential for low-frequency noise reduction in a constrained space.**

**Keywords:** Low-frequency sound absorption, Helmholtz resonator
**I-INCE Classification of Subject Number:** 34

[1] jguoam@connect.ust.hk
[2] aexzhang@ust.hk

## 1. INTRODUCTION

Noise reduction is of great interest in both scientific and engineering fields. Generally, noise reduction techniques can be broadly divided into two main categories: active and passive noise control methods. Active noise control realizes noise reduction by generating a sound wave with equal amplitude and opposite phase to cancel out the noise source, which is quite efficient, however, usually needs complete additional controlling devices [1]. Passive noise control is a reliable and low-cost technique by using sound absorbers, including porous and fibrous materials [2], resonant-type absorbers, such as quarter wavelength (QW) resonator [3], Helmholtz resonator [4], and mirco-perforated plate (MPP) [5, 6]. Porous materials have satisfactory reduction performance for middle and high-frequency ranges, however, perform badly in low-frequency range. Resonant-type absorbers possess satisfying noise reduction performance at the resonance frequency but suffer from the disadvantage of a narrow operation bandwidth around the designed resonant frequency. The devolvement of an absorber with compact dimension possessing the ability of low-frequency noise attenuation over a large frequency range still remains challenging.

In the past few years, the advent of acoustic metamaterials (AMs) provides a promising alternative to the traditional noise reduction strategies for noise elimination. AMs refer to some man-made materials exhibiting exotic properties that cannot be realized using naturally existing materials [7]. To overcome the limitations of a narrow working frequency band and bulky structure existing in conventional sound absorbers for low-frequency noise, a series of AMs-based absorber designs have been proposed. One strategy is to introduce an extended neck to a resonance-type absorber. Li *et al.* [8] proposed to attach tube bundles to the perforated/micro-perforated panel [9]. Similarly, the type of Helmholtz resonator possessing an embedded aperture has also been designed [10, 11]. Simon [12] tested the acoustic performance of this type absorber in an aeroacoustic bench and concluded that a grazing flow has little impact on the impedance value. Although the introduction of extended neck achieves a sub-wavelength sound absorption. However, similar to local-resonance based absorber, their absorption bandwidth is generally narrow just around the designed resonance frequency, thus is insufficient for practical application.

A straightforward approach to the narrow-band problem of the resonance-type resonator is parallelly incorporating multiple inhomogeneous resonators. Many efforts have been dedicated. Sakagami *et al.* [13] combined two different MPP absorbers with different frequency characteristics to achieve a broader absorption frequency range. Afterward, Wang and Huang [14] discussed the distinct acoustic properties and the physical mechanisms of multiple MPP absorber array. Cummer *et al.* [15] tested the two coupled slits of two dimensional (2D) Helmholtz resonators and demonstrated the generation of a hybrid resonance mode. Following this study, the geometric parameters of the absorber with coupled microslits are optimized to enhance low-frequency absorpiotn [16]. These previous works have demonstrated that the enhanced sound absorption performance induced by inhomogeneous impedance discontinuity is valid.

In order to use the excess attenuation caused by inhomogeneously distributed resonators, this work designs and fabricates a sub-wavelength acoustic absorber based on the concept of Helmholtz resonator with extended neck HREN. The absorber is composed of alternating HRENs with different-length extended necks. To analyze the acoustic characteristics of the proposed absorber, an analytical prediction model is

established, which is validated against experimental results measured in an impedance tube. The emphasis of the current research is the noise attenuation benefits caused by the introduction of extended neck to Helmholtz resonator and the alternating distributed HRENs. Both analytical predictions and experimental measurements are included in this study.

## 2. PREDICTION METHOD AND MEASUREMENT SETUP

Figure. 1(a) shows the cross-sectional view of a basic HREN unit (a unit cell), which consists of a Helmholtz resonator with an extended neck, where $d$ and $r_n$ are the thickness and inner radius of neck; $E$ is the length of the extended neck; $l_c$ and $r_c$ are the depth and radius of the backing cavity; $t$ is the thickness of the extended neck. The acoustic characteristics of the resonator are investigated both analytically and experimentally.

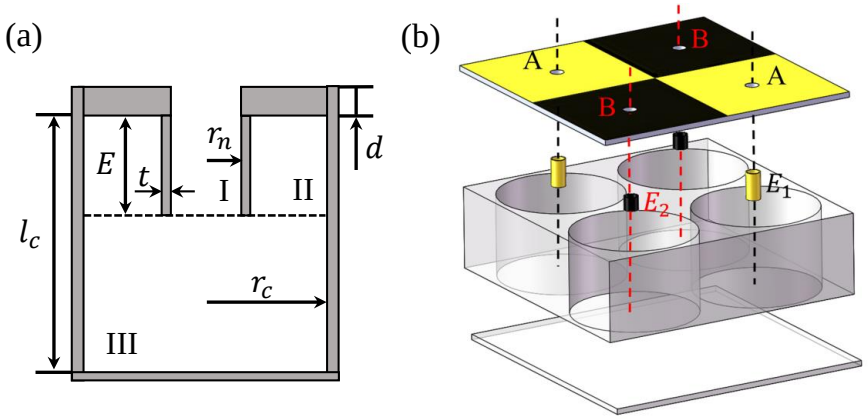


*Figure 1: (a) The cross-sectional view of a Helmholtz resonator with an extended neck. (b) Schematic of a checkerboard absorber composed of alternating resonators A and B with different-length extended necks.*

### 2.2.1. Prediction model

The unit cell shown in Fig. 1(a) can be divided into three regions: the neck region(I), the annular duct (II) and the backing cavity (III). Acoustic wave propagation in a circular tube has been studied theoretically based on Kirchhoff theory [17], in which both viscosity and thermal conductivity in the tube are included. However, the solution of Kirchhoff theory is too complicated and difficult to apply. Based on the equivalent fluid with complex density and complex compressibility, Stinson [18] derived an approximate solution to determine the acoustic propagation characteristics of sound through a circular tube. When the dimensions of the circular neck is much smaller than the wavelength of the incident wave, based on the Stinson's theory, the axial velocity equation in the tube can be expressed as

$$\frac{1}{r}\frac{d}{dr}\left(r\frac{d\psi}{dr}\right)-\frac{i\omega}{\eta}\psi=-\frac{i\omega}{\eta} \tag{1}$$

where $\omega$ and $\rho_0$ refer to the angular frequency and the density of air; $i$ is the imaginary unit; $\eta$ is the viscous coefficient of air; $\psi$ is a generalized variable $\psi = -(i\omega\rho_0/mp)u$, in which $p$, $m$, and $u$ are the sound pressure, the propagation constant and the particle

velocity in the axial direction, respectively. The solution of Equ. 1 is

$$\psi(r) = 1 - J_0\left[r(-i\omega/\eta)^{1/2}\right]/J_0\left[r_w(-i\omega/\eta)^{1/2}\right], \tag{2}$$

where $J_n(n = 0, 1)$ is the $n_{th}$ order Bessel function of the first kind. Function $F(\eta)$ is defined by the average of $\psi$ of the cross section of the circular tube:

$$F(\eta) = \langle\psi\rangle = 1 - 2(-i\omega/\eta)^{-1/2}G\left[r_w(-i\omega/\eta)^{1/2}\right]/r_w \tag{3}$$

where $r_w$ is the radius of the tube; $G$ is defined by $G(\xi) = J_1(\xi)/J_0(\xi)$. The complex density $\rho_e$ and the complex compressibility $C_e$ functions are obtained by

$$\rho_e(\omega) = \rho_0/F(\nu), \tag{4}$$

$$C_e(\omega) = (1/\gamma P_0)\left[\gamma - (\gamma - 1)F\left(\nu'/\gamma\right)\right], \tag{5}$$

where $P_0$ and $\gamma$ are the pressure of air and the ratio of specific heats; $\nu = \mu/\rho_0$ and $\nu' = \kappa/\left(\rho_0 C_v\right)$ in which $\mu$, $\kappa$ and $C_v$ are the viscosity of air, the thermal conductivity of air and the specific heat at constant volume. The bulk modulus function is obtained by $K_e(\omega) = 1/C_e(\omega)$. The effective impedance and the effective wavenumber of the circular tube are calculated by

$$Z_e(\omega) = \sqrt{\rho_e(\omega)K_e(\omega)}/S, \tag{6}$$

$$k_e(\omega) = \omega\sqrt{\rho_e(\omega)/K_e(\omega)}, \tag{7}$$

where $S$ is the surface area of the circular tube. Consider a plane wave normally impinge on a unit cell. On the basis of the continuities of pressure and volume velocity, the acoustic properties in the unit cell can be studied by the transfer matrix method

$$\begin{bmatrix} p_{\text{in}} \\ u_{\text{in}} \end{bmatrix} = T_t \begin{bmatrix} p_{\text{out}} \\ u_{\text{out}} \end{bmatrix} = \begin{bmatrix} T_{11} & T_{12} \\ T_{21} & T_{22} \end{bmatrix} \begin{bmatrix} p_{\text{out}} \\ u_{\text{out}} \end{bmatrix}, \tag{8}$$

where $p_{\text{in}}, u_{\text{in}}$ are the incoming pressure and normal volume velocity; $p_{\text{out}}, u_{\text{out}}$ are the pressure and normal volume velocity on the end wall of the backing cavity ($u_{\text{out}} = 0$); $T_{11}$, $T_{12}$, $T_{21}$ and $T_{22}$ are the elements of the total transfer matrix $T_t$. Note that $T_t$ can be calculated by three different regions of the unit cell, i.e., the neck (I), the annular duct (II) and the backing cavity (III). The transfer matrices of these three regions can be written as

$$T_n = \begin{bmatrix} \cos(k_n l_n) & iZ_n \sin(k_n l_n) \\ i\sin(k_n l_n)/Z_n & \cos(k_n l_n) \end{bmatrix}, \tag{9}$$

$$T_a = \begin{bmatrix} 1 & 0 \\ i\tan(k_a E)/Z_a & 1 \end{bmatrix}, \tag{10}$$

$$T_c = \begin{bmatrix} \cos(k_c D) & iZ_c \sin(k_c D) \\ i\sin(k_c D)/Z_c & \cos(k_c D) \end{bmatrix}, \tag{11}$$

where $Z_n$, $Z_a$ and $Z_c$ are the effective impedance of the neck, the annular duct and the backing cavity respectively; $k_n$, $k_a$ and $k_c$ are the corresponding complex wave number; $l_n = d + E$ is the length of the neck. Note that the annular duct region is treated as a side branch in the transfer matrix method. Considering that the radius of the extended neck is much smaller than that of the backing cavity, it is reasonable to take $Z_a \approx Z_c$ and $k_a \approx k_c$.

There is an abrupt change of neck cross-section at the connection between neck and free space, and the discontinuity also occurs at the connection between the neck and cavity, which will educe sound radiation. The radiation effect can be represented by an increase in the equivalent length of the neck, i.e., end correction. For two different circular cross sections, Karal [19] derived the expression of end correction. Taking the discontinuity between neck and cavity for instance, the end correction can be expressed as

$$\delta_{n-c} = 4r_n \sum_{m=1}^{\infty} \frac{J_1^2\left(x_m r_n / r_c\right)}{\left(x_m r_n / r_c\right)\left[x_m J_0\left(x_p\right)\right]^2}, \tag{12}$$

where $x_m$ is the $m^{\text{th}}$ root of $J_1(x_m) = 0$. The end correction due to the radiation effect induced by the discontinuity from free space to neck $\delta_{f-n}$ can also be calculated straightforward (note that the effective radius of free space is used). The effective length of the neck used in Equ. 9 is increased to $l_n' = l_n + \delta_{n-c} + \delta_{f-n}$.

By connecting $T_n$, $T_a$ and $T_c$, one can obtain the overall transfer matrix of a unit cell

$$T_t = T_n T_a T_c. \tag{13}$$

Due to the rigid back of the unit cell, the surface impedance of the unit cell can be obtained based on the overall transfer matrix

$$Z = \frac{\cos(k_n l_n)\cos(k_c l_c) - Z_n \cos(k_c l_c)\sin(k_n l_n)\tan(k_a E)/Z_a - Z_n \sin(k_n l_n)\sin(k_c l_c)/Z_c}{(i/Z_n)\sin(k_n l_n)\cos(k_c l_c) + (i/Z_a)\cos(k_n l_n)\cos(k_c l_c)\tan(k_a E) + (i/Z_c)\sin(k_c l_c)\cos(k_n l_n)}. \tag{14}$$

For a combination of parallel assembled HRENs, as shown in Fig. 1(b), the overall impedance $Z_t$ can be calculated by as follows

$$\frac{S_t}{Z_t} = \sum_{i=1}^{N} \frac{S_i}{Z_i}, \tag{15}$$

where, $N$ is the total number of HRENs; $S_i$ and $Z_i$ are the area and the surface impedance of $i$-th HREN; overall area $S_t = \sum_{i=1}^{N} S_i$. Once the surface impedance of the resonator is obtained, the reflection coefficient can be evaluated as follows:

$$R = \frac{4\mathrm{Re}(Z_t/\rho_0 c_0)}{\mathrm{Re}(Z_t/\rho_0 c_0)^2 + \mathrm{Im}(Z_t/\rho_0 c_0)^2}. \tag{16}$$

Then the sound absorption coefficient is determined by $\alpha = 1 - |R|^2$. The requirement for total absorption (i.e., absorption coefficient reaches unity) is to satisfy the impedance matching condition between the background medium and the absorber, i.e., $\mathrm{Re}(Z) = 1$ and $\mathrm{Im}(Z) = 0$.

### 2.2.2. Measurement setup

To verify the accuracy of the prediction model, the absorption characteristics of HREN are also measured experimentally using an impedance tube with a square cross-section, as shown in Fig. 2(a). The impedance tube is fabricated by using acrylic plates with a thickness of 20 mm. The dimension of the impedance tube is 50 mm×50 mm, thus the plane wave cutoff frequency of the tube is 3560 Hz. A loudspeaker is placed at one end of the impedance tube to generate a random sound source (white noise), and a test sample

is placed at the other end of the impedance tube. Two 1/4-inch microphones (Brüel & Kjr type-2670) are flush-mounted separately between the loudspeaker and the test sample, with a distance of 30 mm. Based on the transfer function between two microphones (more details can be found in ISO 10534-2 [20].), the reflection and absorption coefficients of the test sample can be obtained.

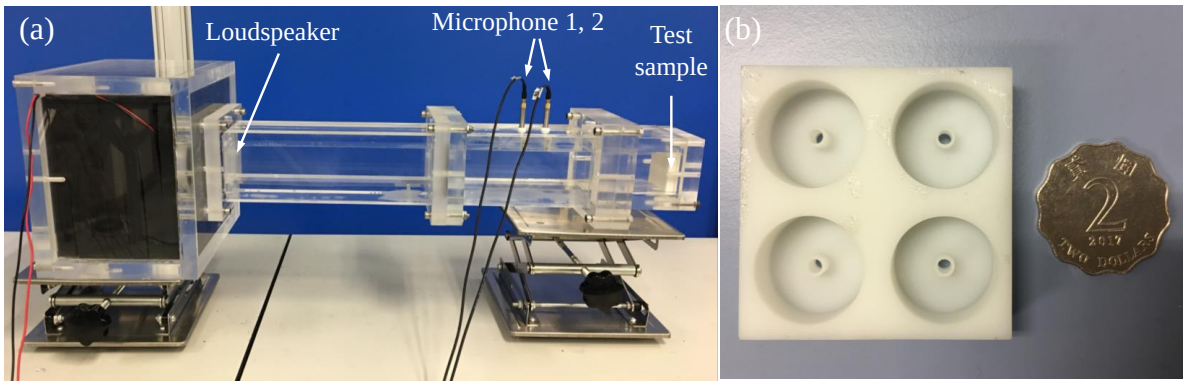


*Figure 2: (a) Schematic of the impedance tube used for measurements. (b) A bottom view of a 3D-printing test sample with $E = 4$ mm.*

## 3. RESULTS AND DISCUSSION

### 3.3.1. Uniform HREN

We first analyze the behavior of the uniform HREN absorber. Consider the dimension of the rectangular impedance tube ($50 \times 50$ mm) used in measurements, the cavity radius of the HREN unit is set as $r_c = 10$ mm. Other geometric parameters of the HREN unit are designed as $r_n = 1.4$ mm, $d = 2.5$ mm, $l_c = 10.0$ mm, and $t = 0.6$ mm. The effect of the key structure parameter $E$ on the absorption performance of HREN is studied. A bottom view of a test sample with $E = 4$ mm is shown in Fig.2(b), which consists of four uniform HRENs. The test sample is fabricated by using a 3D printing technique. The fabricated material is photosensitive resin, with a density of 1210 kg/m$^3$ and with a sound speed of 1024 m/s. They are much larger than that of air, making it reasonable to treat the material as an acoustically rigid medium.

Fig.3(a) gives the sound absorption comparison of Helmholtz resonators with different extended necks with $E$=0.0, 2.0, 4.0, and 6.0 mm. From Fig. 3(a), the maximum absorption values of HRENs with $E$=0.0, 2.0, 4.0, and 6.0 mm are 0.95, 0.96, 0.99 and 0.94 at 1093.8, 927.3, 805.7 and 720.2 Hz, respectively in experiments, and those corresponding predicted results are 0.88, 0.95, 0.99 and 0.99 at 1098.9, 918.4, 804.5 and 725.7 Hz, respectively. Good agreement between analytical prediction and experimental results is shown in Fig.3(a) in terms of the location and value of the maximum absorption, which indicates the prediction method is capable of predicting the absorption performance of HREN. Some small deviations between predictions and measurements may be attributed to the imperfection in the manufacture of test sample, experimental errors such as the gap between the test sample and impedance tube and the imperfect seal of microphones. The underlying physics for maximum absorption at the resonance frequency is that: a viscous dissipation and a thermal dissipation process are educed in the viscous and thermal boundary layers, because of the severe oscillation of air in the neck at resonance frequency [21]. From Fig. 3(a), apparently, the introduction of

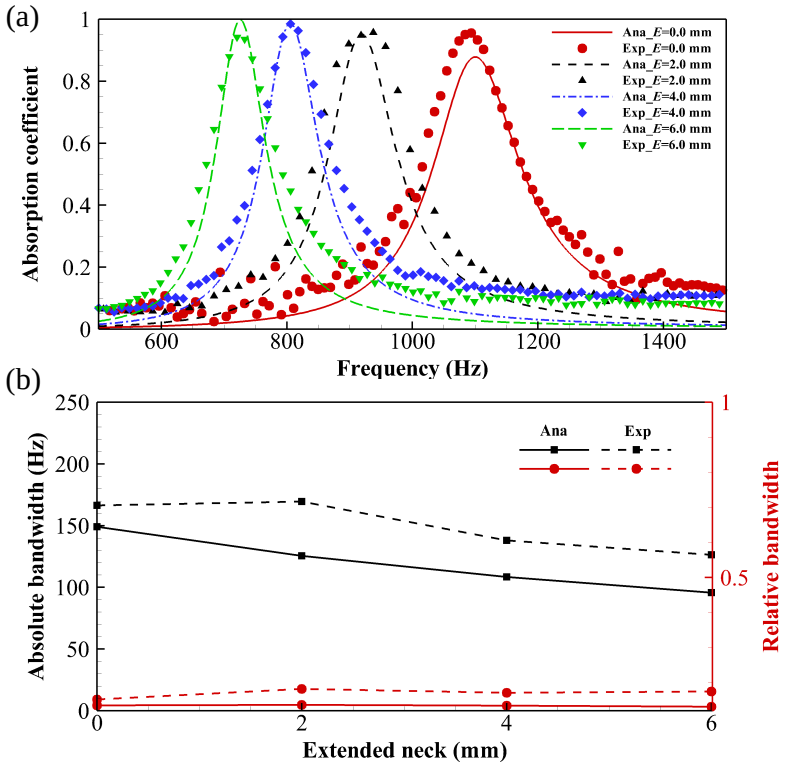


*Figure 3: (a) Sound absorption comparison of uniform absorbers with different extended necks ($E = 0.0, 2.0, 4.0, 6.0$ mm) as a function of frequency. (b) Relative absorption bandwidth and absolute absorption bandwidth as a function of the length of the extended neck.*

extended neck shifts the resonance frequency (i.e., absorption peak) to a lower frequency. In other words, HREN achieves a lower frequency sound absorption compared with the conventional Helmholtz resonator with an identical thickness, which is consistent with the previous works [9, 12]. The feature of resonance frequency shifting makes HREN a promising low-frequency sound absorber in a limited space. Take HREN with E=6.0 mm for instance, the overall thickness is 12.5 mm, which is approximately 1/40 of the wavelength of the resonance frequency. Figure. 3(a) also shows that with an increase in the length of the extended neck, there is a decrease in the frequency band of absorption. To quantify the absorption bandwidth of HREN, two variables, i.e., absolute absorption bandwidth $\Delta f$ and relative absorption bandwidth $\Delta f/f_0$ are defined, where $\Delta f$, $f_0$ are the frequency width of half-absorption and the resonance frequency, respectively. Figure. 3(b) shows the relationship between $E$ and $\Delta f$, $\Delta f/f_0$ for HREN. It is found that increasing of the length of extended neck narrows the absolute absorption bandwidth, but the relative absorption bandwidth is independent of the length of the extended neck. In summary, the resonance frequency of the resonator can be easily adjusted by carefully varying the length of the extended neck, while the total absorption is preserved.

### 3.3.2. Checkerboard absorber

#### 3.2.1 Design principle

Section. 3.1 has demonstrated that HREN reduces the resonance frequency obviously, however, an isolated resonator structure is inherent narrow-band. To broaden the

absorption bandwidth, the strategy is to incorporate multiple HRENs with different length of extended neck. As shown in Fig. 1(b), a checkerboard absorber based on the concept of HREN is designed, which is composed of alternating resonators A and B with different extended neck lengths $E_1$ and $E_2$ respectively. The absorption band can be tuned by assigning different $E_1$ and $E_2$. Note that in this work a four-resonators absorber ($2 \times 2$) is used in experimental measurements.

### 3.2.2 A dual-band absorber

When the difference between resonance frequencies of resonators A and B is large, i.e., two largely dissimilar resonators are used, a dual-band absorber is obtained. Take a sample with $E_1 = 1$ mm and $E_2 = 5$ mm for instance. The absorption spectrum of the dual-band absorber is shown in Fig. 4(a). For comparison, the absorption spectra of two corresponding uniform HRENs are also presented. Apparently, a dual resonance

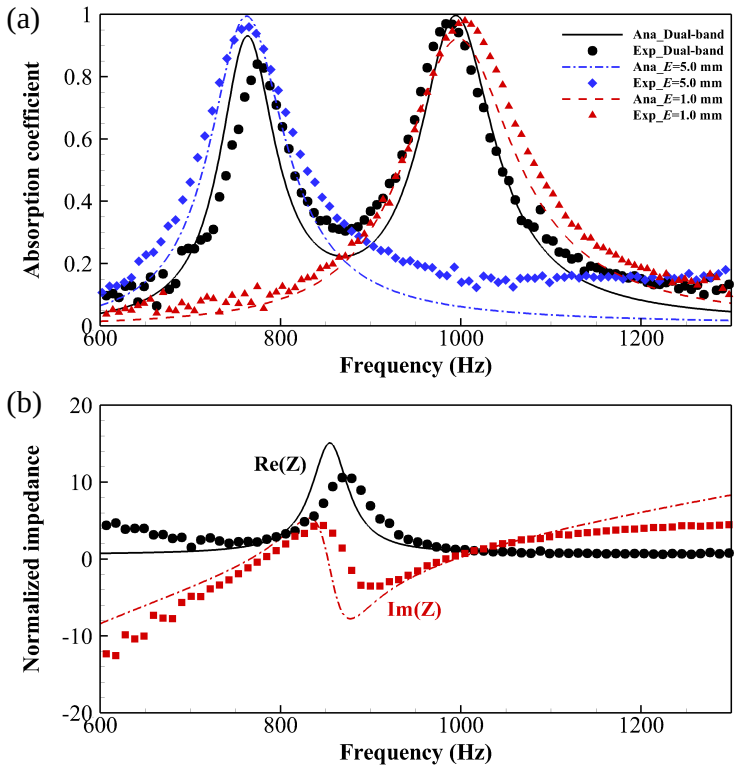


*Figure 4: (a) Sound absorption performance of a dual-band absorber. (b) The predicted (lines) and measured (symbols) real and imaginary parts of the normalized impedance of the dual-band absorber (by air characteristic impedance).*

phenomenon is induced by the dual-band absorber. Two discrete absorption peaks at 777.8 Hz and 987.0 Hz with the absorption of 0.86 and 0.97 are observed in experiments. These values are in generally good agreement with the predicted results: 764.2 Hz and 994.5 Hz with the absorption of 0.93 and 0.99. Two absorption peaks of the dual-band absorber just correspond to those of the two uniform HRENs with $E_1 = 5$ mm and $E_2 = 1$ mm (760.9 Hz and 1004.5 Hz in experiments), i.e., little frequency shift is observed. In addition, the measured absolute absorption bandwidth of these two peaks are 72.3 Hz (from 743.2 to 814.5 Hz) and 116.1 Hz (from 929.9 to 1046.0 Hz), which are also correspond to the inhomogeneous HRENs. The good coincidences indicate that

the HRENs in the dual-band absorber behave as discrete resonances, lacking of coupling effect. The underlying mechanism is that due to the resonance frequencies of resonators with $E_1 = 1$ mm and $E_2 = 5$ mm are largely different, the difference of the reflected energy between adjacent resonators at each resonance frequency is pretty large, thus the coupling between resonators becomes quite weak. In addition, for this dual-band absorber, the overall thickness is about 1/35 of the wavelength at the first absorption peak.

To further investigate acoustic characteristics of the absorber, Fig. 4(b) gives the normalized impedance (by the characteristic impedance of air) of the dual-band absorber, note that both the real and imaginary parts are included. From Fig. 4(b), the trends of the impedance curves are predicted well. The measured impedance values at two absorption peaks (777.8 Hz and 987.0 Hz) are $2.20 - 0.09i$ and $1.39 + 0.11i$. They are close to the requirement of impedance matching to the background medium, i.e., $1 + 0i$, especially for the second absorption peak.

### 3.2.3 A wide-bandwidth absorber

By adjusting the resonance frequencies of alternative resonators to be close to each other, a wide-bandwidth absorber is achieved due to the strong coupling effect between adjacent HRENs. Here design a sample with $E_1 = 2.2$ mm and $E_2 = 3.45$ mm. The measured and predicted sound absorption coefficients of the wide-bandwidth absorber are

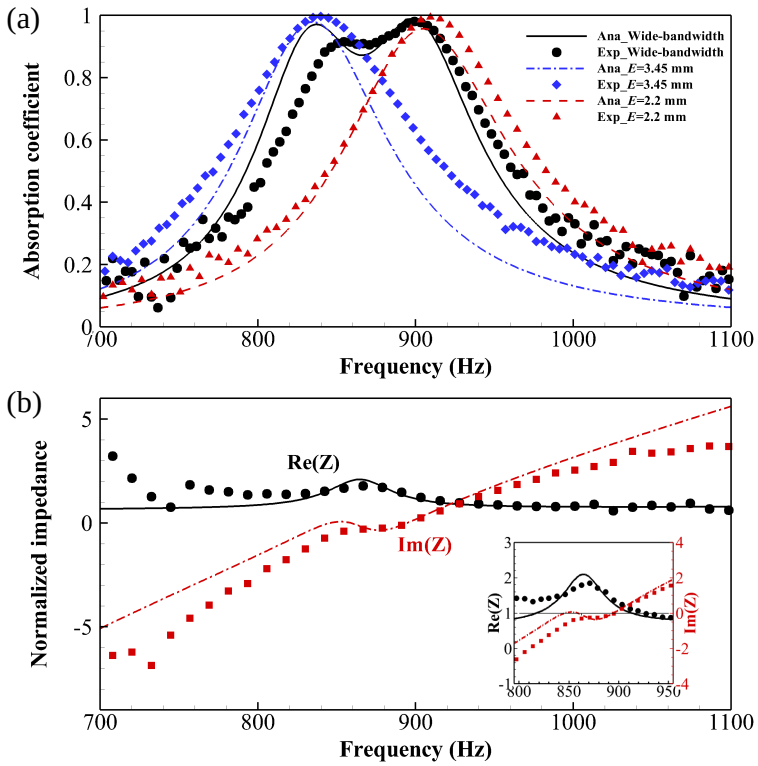


*Figure 5: (a) Sound absorption performance of the proposed checkerboard absorber. (b) The predicted (lines) and measured (symbols) real and imaginary parts of the normalized impedance of the broadband absorber (by air characteristic impedance).*

given in Fig. 5(a). For comparison, the absorption curves of the corresponding uniform HRENs are also presented. The normalized impedance of the proposed absorber is shown

in Fig. 5(b). It can be seen from Fig. 5(a) and (b) that a generally good agreement is found between predictions and measurements.

From Fig. 5(a), the resonance frequencies of HRENs with $E_1$ = 2.2 mm and $E_2$ = 3.45 mm are 909.4 Hz and 839.8 Hz in experiments (906.1 Hz and 834.3Hz in predictions). Good absorption performance is consistently maintained in the transition band between two absorption peaks induced by two uniform HRENs. The measured absolute bandwidth of the wide-bandwidth absorber is 158.4 Hz (from 804.0 to 962.4 Hz), which is wider than these of the two uniform HRENs: 139.2 Hz (from 843.8 to 983.0 Hz) and 148.8 Hz (from 771.7 to 920.5 Hz). In addition, the merit of absorption bandwidth expansion by the wide-bandwidth absorber is more obvious for quasi-perfect absorption performance (the absorption coefficient $>$ 0.90). The measured quasi-perfect absorption bandwidth asserted by the wide-bandwidth absorber is 71.5 Hz in the frequency range of 847.2 Hz to 918.7 Hz, which is 1.63 times and 1.47 times wider than these of the corresponding uniform HRENs, respectively. Correspondingly, it can be seen that the impedance matching condition is nearly satisfied in the quasi-perfect absorption band from Fig. 5(b), resulting in a little reflection. Hence, the wide-bandwidth absorber performs better as a whole rather than the corresponding uniform HRENs in terms of the sound absorption bandwidth. The improvements in the absorption bandwidth can be attributed to the coupling of inhomogeneous HRENs in the checkerboard absorber. What's more, the thickness of the wide-bandwidth absorber is just about 1/32 of the start frequency of the quasi-perfect absorption. Note that the thickness of absorber can be further reduced if an optimization on the geometric parameters of the absorber is conducted.

## 4. CONCLUSION

Based on Helmholtz resonator with extended neck (HREN), we propose a thin low-frequency acoustic absorber composed of checkerboard HRENs with different-length extended necks, in an attempt to achieve a dual-band or wide-bandwidth absorption. By coupling the equivalent medium method and the transfer matrix method, an analytical prediction model is derived to capture the sound absorption performance of absorber. Good agreement is attained between analytic predictions and experimental measurements, verifying the accuracy of the prediction model. Results indicate that the introduction of extended neck shifts the resonance frequency to a lower frequency, making the absorber possess a thin thickness feature. When the alternating resonators in the checkerboard absorber are dissimilar largely, a dual-band absorber is obtained. The dual absorption peaks just follow the corresponding uniform HRENs. To achieve broadband dissipation, a wide-bandwidth absorber composed of two fully coupled HRENs is designed. A quasi-perfect absorption property (the absorption coefficient above 0.9) at a relatively wide frequency band ranging from 847.2 Hz to 918.7 Hz is attained. The features of thin thickness and adjustable wide absorption bandwidth make the proposed absorber hold promising potential for noise attenuation in practical applications.

## 5. ACKNOWLEDGEMENTS

Part of this work was supported by the National Science Foundation of China (11772282).

## 6. REFERENCES


[1] Sen M Kuo and Dennis R Morgan. Active noise control: a tutorial review. *Proceedings of the IEEE*, 87(6):943–973, 1999.

[2] Jean Allard and Noureddine Atalla. *Propagation of sound in porous media: modelling sound absorbing materials 2e*. John Wiley & Sons, 2009.

[3] Tristan Cambonie, Fulbert Mbailassem, and Emmanuel Gourdon. Bending a quarter wavelength resonator: Curvature effects on sound absorption properties. *Applied Acoustics*, 131:87–102, 2018.

[4] Uno Ingard. On the theory and design of acoustic resonators. *The Journal of the acoustical society of America*, 25(6):1037–1061, 1953.

[5] Dah-You Maa. Potential of microperforated panel absorber. *the Journal of the Acoustical Society of America*, 104(5):2861–2866, 1998.

[6] Cheng Yang, Li Cheng, and Jie Pan. Absorption of oblique incidence sound by a finite micro-perforated panel absorber. *The Journal of the Acoustical Society of America*, 133(1):201–209, 2013.

[7] Jingwen Guo, Xin Zhang, Yi Fang, and Ryu Fattah. Reflected wave manipulation by inhomogeneous impedance via varying-depth acoustic liners. *Journal of Applied Physics*, 123(17):174902, 2018.

[8] Noe Jiménez, Weichun Huang, Vicent Romero-García, Vincent Pagneux, and J-P Groby. Ultra-thin metamaterial for perfect and quasi-omnidirectional sound absorption. *Applied Physics Letters*, 109(12):121902, 2016.

[9] Dengke Li, Daoqing Chang, and Bilong Liu. Enhancing the low frequency sound absorption of a perforated panel by parallel-arranged extended tubes. *Applied Acoustics*, 102:126–132, 2016.

[10] Jingwen Guo, Xin Zhang, Yi Fang, and Ryu Fattah. Manipulating reflected acoustic wave via helmholtz resonators with varying-length extended necks. *Journal of Applied Physics*, 124(10):104902, 2018.

[11] Sibo Huang, Xinsheng Fang, Xu Wang, Badreddine Assouar, Qian Cheng, and Yong Li. Acoustic perfect absorbers via spiral metasurfaces with embedded apertures. *Applied Physics Letters*, 113(23):233501, 2018.

[12] Frank Simon. Long elastic open neck acoustic resonator for low frequency absorption. *Journal of Sound and Vibration*, 421:1–16, 2018.

[13] Kimihiro Sakagami, Yoshiki Nagayama, Masayuki Morimoto, and Motoki Yairi. Pilot study on wideband sound absorber obtained by combination of two different microperforated panel (mpp) absorbers. *Acoustical science and technology*, 30(2):154–156, 2009.

[14] Chunqi Wang and Lixi Huang. On the acoustic properties of parallel arrangement of multiple micro-perforated panel absorbers with different cavity depths. *The Journal of the Acoustical Society of America*, 130(1):208–218, 2011.

[15] Junfei Li, Wenqi Wang, Yangbo Xie, Bogdan-Ioan Popa, and Steven A Cummer. A sound absorbing metasurface with coupled resonators. *Applied Physics Letters*, 109(9):091908, 2016.

[16] Honggang Zhao, Yang Wang, Jihong Wen, Yiu Wai Lam, and Olga Umnova. A slim subwavelength absorber based on coupled microslits. *Applied Acoustics*, 142:11–17, 2018.

[17] John William Strutt Baron Rayleigh. *The theory of sound*, volume 2. Macmillan, 1896.

[18] Michael R Stinson. The propagation of plane sound waves in narrow and wide circular tubes, and generalization to uniform tubes of arbitrary cross-sectional shape. *The Journal of the Acoustical Society of America*, 89(2):550–558, 1991.

[19] FC Karal. The analogous acoustical impedance for discontinuities and constrictions of circular cross section. *The Journal of the Acoustical Society of America*, 25(2):327–334, 1953.

[20] ISO. Acoustics - determination of sound absorption coefficient and impedance in impedances tubes - part 2: Transfer-function method. ISO 10534-2, 1998.

[21] Tristan Cambonie and Emmanuel Gourdon. Innovative origami-based solutions for enhanced quarter-wavelength resonators. *Journal of Sound and Vibration*, 434:379–403, 2018.